JGR Space Physics

RESEARCH ARTICLE
10.1029/2019JA027667

Evolution of High-Speed Jets and Plasmoids Downstream of the Quasi-Perpendicular Bow Shock

O. Goncharov[1], H. Gunell[1,2], M. Hamrin[1], and S. Chong[1]

[1]Department of Physics, Umeå University, Umeå, Sweden, [2]Royal Belgian Institute of Space Aeronomy, Brussels, Belgium

Key Points:
- The jets grow larger and slower as they move away from the bow shock
- The deceleration of jets and fast plasmoids in the quasi-perpendicular magnetosheath is twice as fast as in the quasi-parallel magnetosheath
- Jets propagate deeper into the magnetosheath for smaller angles between the interplanetary magnetic field and the bow shock normal

Correspondence to:
O. Goncharov,
oleksandr.goncharov@umu.se

Citation:
Goncharov, O., Gunell, H., Hamrin, M., & Chong, S. (2020). Evolution of high-speed jets and plasmoids downstream of the quasi-perpendicular bow shock. *Journal of Geophysical Research: Space Physics*, *125*, e2019JA027667. https://doi.org/10.1029/2019JA027667

Received 25 NOV 2019
Accepted 13 MAY 2020
Accepted article online 19 MAY 2020

Abstract Plasma structures with enhanced dynamic pressure, density, or speed are often observed in Earth's magnetosheath. We present a statistical study of these structures, known as jets and fast plasmoids, in the magnetosheath, downstream of both the quasi-perpendicular and quasi-parallel bow shocks. Using measurements from the four Magnetospheric Multiscale (MMS) spacecraft and OMNI solar wind data from 2015–2017, we present observations of jets during different upstream conditions and in the wide range of distances from the bow shock. Jets observed downstream of the quasi-parallel bow shock are seen to propagate deeper and faster into the magnetosheath and on toward the magnetopause. We estimate the shape of the structures by treating the leading edge as a shock surface, and the result is that the jets are elongated in the direction of propagation but also that they expand more quickly in the perpendicular direction as they propagate through the magnetosheath.

Plain Language Summary The solar wind is a stream of charged particles continuously emitted from the upper atmosphere of the Sun. When it approaches Earth, it is slowed down and creates the bow shock. The region with high temperature and lower speed, downstream of the bow shock is called the magnetosheath. From time to time, plasma jets with speeds close to the solar wind speed are observed in this magnetosheath. They are thought to be formed at the bow shock, which is the boundary between the magnetosheath and the solar wind. In this article, we use data obtained by the four MMS spacecraft, while they passed through the magnetosheath, in a statistical study of the properties of the jets. We have found that they slow down as they move through the magnetosheath and that, in the beginning, they are elongated in the direction of their motion, but also that they expand to become rounder as they move along.

1. Introduction

The bow shock is the boundary at which the speed of the solar wind abruptly drops as it approaches Earth. Downstream of the shock, in the magnetosheath, the plasma is denser and hotter than in the unperturbed solar wind, and the magnetic field is stronger than the interplanetary magnetic field (IMF). The structure of the bow shock depends to a large extent on whether the IMF is close to parallel or perpendicular to the shock normal. This also affects the particle populations through processes that lead to reflection of particles, the formation of a foreshock, and the wave activity in the vicinity of the shock. For small angles between the bow shock normal and the IMF ($\theta_{Bn} < 45°$), the shock is quasi-parallel, and for large angles ($\theta_{Bn} > 45°$), it is known as quasi-perpendicular.

Ions reflected at the quasi-parallel shock travel as beams through the upstream plasma, generating waves in the foreshock region through wave-particle interaction (e.g., Wilson et al., 2013). This is also where short large-amplitude magnetic structures (SLAMS) have been observed (Schwartz et al., 1992). The quasi-parallel bow shock is replaced repeatedly by newly forming shocks, which leads to strong fluctuations also in the magnetosheath downstream (Blanco-Cano et al., 2006a, 2006b; Burgess, 1989; Scholer & Burgess, 1992; Schwartz et al., 1992).

During the last two decades, a number of authors have reported observations of plasma entities that stand out from the surrounding magnetosheath by having either an enhanced density, speed, or both. A few different terms have been used to denote these structures, for example, "magnetosheath dynamic pressure enhancements" (Archer & Horbury, 2013), "density enhancements" (Gutynska et al., 2015), "transient flux enhancements" (Němeček et al., 1998), "antisunward high-speed jets" (HSJ) (Plaschke et al., 2013), "supermagnetosonic subsolar magnetosheath jets" (Hietala et al., 2012), "high kinetic energy density

Table 1
Summary of Definitions and Selection Criteria Used Here and in Some of the Previously Published Articles

Denomination	Criterion	Reference
Dynamic pressure enhancement	At least a 100% increase of P_d above a 20 min running average	Archer and Horbury (2013)
Plasmoid	At least a 100% increase of $\|v_x\|$ above a 10-min average after s/c magnetosheath entry, $v_x < 0$	Gunell et al. (2014)
Embedded plasmoid	At least a 50% increase of n_e and less than 10% increase of v above a 500-s running average	Karlsson et al. (2012)
Fast plasmoid	At least a 50% increase of n_e and at least 10% increase of v above a 500-s running average	Karlsson et al. (2012)
Diamagnetic plasmoid	At least a 50% increase of n_e (30% in solar wind) and $\Delta B < 0$ (ΔB: maximum deviation from a 5–10-min average before or after plasmoid encounter)	Karlsson et al. (2015)
Paramagnetic plasmoid (subset of magnetosheath jets)	At least a 50% (30% in solar wind) increase of n_e and $\Delta B > 0$ (ΔB defined as above)	Karlsson et al. (2015)
Antisunward high-speed jet	$P_{dx} > 0.25\ P_{dsw}$ throughout plasmoid and max (P_{dx}) $> 0.5\ P_{dsw}$	Plaschke et al. (2013)
Jet	$P_{dx} > 0.4\ P_{dsw}$ throughout plasmoid and max (P_{dx}) $> P_{dsw}$ and max (P_{dx}) at least twice a 20-min running average	This work
Fast plasmoid	Same as jet condition on P_{dx} in this work and a 10% increase of v above a 20-min running average	This work

plasma jets" (Savin et al., 2008), "large-scale jet" (Dmitriev & Suvorova, 2015), and "super fast plasma streams" (Savin et al., 2012). However, Gunell et al. (2014) used the term "plasmoid" to describe velocity structures with the typical scales on the order of 1 Earth radius (R_E). The same term was used by Karlsson et al. (2012) to investigate enhancements in the magnetosheath density. In spite of the disparate terminology, one could, in a general sense, treat these terms as synonyms. However, the detailed properties of the entities observed do depend on precise definitions and selection criteria. We shall use the term "jet" for all the plasma entities in our data set and "fast plasmoid" for the subset whose elements also show a speed increase of 10% or more. The criteria used in this work and in some of the previously published studies are summarized in Table 1.

Statistical studies have shown that jet occurrence is almost exclusively controlled by the angle between the IMF and the Earth-Sun line (cone angle), while other solar wind parameters or their variability only play a minor role. The jets are predominantly observed when this cone angle is small, that is to say, downstream of the quasi-parallel shock (Archer & Horbury, 2013; Hietala & Plaschke, 2013; Plaschke et al., 2013). It was also found that 97% of the observed jets can be formed locally at the bow shock—as opposed to upstream in the solar wind—by ripples that appear on the shock when it is quasi-parallel (Hietala & Plaschke, 2013).

In contrast to the quasi-parallel bow shock, the quasi-perpendicular shock is well-defined, with a relatively thin ion ramp (thickness of several thermal gyroradii), and the magnetosheath is less turbulent downstream of the quasi-perpendicular than the quasi-parallel bow shock. The reflected ions gain enough energy to pass through the shock front from only one full gyromotion, and there is not enough time for waves to grow. Nevertheless, locally generated waves have been observed in the downstream region (Goncharov et al., 2014; Hoilijoki et al., 2016; Lembège et al., 2004; Mazelle et al., 2003; Němeček et al., 2013; Ofman et al., 2009; Ofman & Gedalin, 2013; Soucek et al., 2015; Yang et al., 2012; Yang, Lu & Wang, 2009; Yang, Lu, Lembège et al., 2009). Recently, shock ripples have been observed at quasi-perpendicular bow shock (Johlander et al., 2016). Johlander et al. (2018) concluded that the shock ripples propagated along the shock surface as quasi-periodic fluctuations with Alfvénic wave-like structure. Gutynska et al. (2015) performed an analysis of the wave properties for understanding the nature of the magnetosheath plasma structures and concluded that events with significant density and pressure enhancements are fast magnetosonic waves. Global electromagnetic hybrid simulations (Omidi et al., 2014) suggest that jets that have been formed at the quasi-parallel bow shock for small IMF cone angles may extend into the quasi-perpendicular magnetosheath at the flanks.

On the other hand, at the flanks of the magnetosheath, the magnetosheath plasma stream is itself supermagnetosonic, and bow shock ripples would not necessarily create discernible jets. Archer and Horbury (2013) reported that jets become less common toward the flanks. However, Karlsson et al. (2015) observed density enhancements throughout the dayside flanks. Despite the increasing number of observational studies, the jet formation mechanism remains an open question. Karlsson et al. (2015) suggested that SLAMS (Schwartz, 1991; Schwartz et al., 1992) could transform into jets when traveling through the bow shock. It was found in a global hybrid-Vlasov simulation that a jet can be created through the interaction between the bow shock and a SLAMS-like structure passing through it (Palmroth et al., 2018).

In this paper, we investigate jets in the quasi-perpendicular magnetosheath. We will compare their evolution and relation to upstream parameters, with previous statistical studies of jets, downstream of the quasi-parallel bow shock. We use data from the four Magnetospheric Multiscale (MMS) spacecraft (Burch et al., 2016), orbiting in the magnetosheath and bow shock region, and NASA OMNI high-resolution solar wind data (King & Papitashvili, 2005), gathered during the years 2015–2017. We compare several models of the jet formation mechanism and provide quantitative predictions of jet propagation toward the magnetopause.

2. Data Set and Methodology

From October 2015, the orbits of MMS spacecraft cover a broad region of the magnetosheath. Our visual inspection of the ion energy spectra, plasma, and magnetic field signatures in MMS Quicklook plots (https://lasp.colorado.edu/mms/sdc/public/plots/quicklook) excluded the magnetosphere and solar wind parts. We used fast survey mode resolution of the magnetic field (16 Hz) and plasma (4.5 s/sample) measurements (Pollock et al., 2016; Russell et al., 2014). The electric current density, $\boldsymbol{J}$, was estimated by the curlometer method from the four MMS magnetic field data (Dunlop et al., 2002; Paschmann & Schwartz, 2000).

Different physical parameters have been used to identify jets previously. The choice of parameters often affect the nomenclature and the numbers of selected events. The best choice of an identification criterion to use in future studies is still under debate, and it will depend on the particular science questions and the availability of measurements. In this work, we compare several criteria, which have been adopted from previous observational studies. Each selected interval of the magnetosheath region was automatically analyzed to look for the enhancements in the antisunward (negative X component) velocity (Gunell et al., 2014; Hietala et al., 2009, 2012). All events were visually inspected and compared with the Plaschke et al. (2013) (P13) identification criterion, defined by the ratio of the magnetosheath dynamic pressure in the X direction ($P_{\mathrm{dx}} = \rho \cdot V_x^2$) to the upstream solar wind dynamic pressure ($P_{\mathrm{dsw}} = \rho \cdot V_{\mathrm{sw}}^2$), where ρ is the mass density. According to their selected criterion, the jet is a region where $P_{\mathrm{dx}} > 0.25 \cdot P_{\mathrm{dsw}}$ with a maximum value higher than $0.5 \cdot P_{\mathrm{dsw}}$. Furthermore, this criterion would only be applicable in the subsolar region of the magnetosheath since the magnetosheath velocity in the flanks increases with respect to the solar wind velocity, and this inequality would be satisfied almost all the time. A summary of these criteria can be viewed in Table 1.

A comparative analysis of different criteria by Plaschke et al. (2018) predicted that the Archer and Horbury (2013) (AH13), P13, and Karlsson et al. (2012, 2015) (K12) criteria identified the most events and that of these, the lower threshold of AH13 provide the highest number of events. However, the actual overlap in the three definitions, which were applied to the Archer and Horbury (2013) survey with no further assumptions, showed that just under 3% of all identified data points are common to them all. About 60% of all observations identified by K12 criterion also satisfy one of the other two definitions. On the other hand, about half of the samples identified by P13 are not satisfied by the other two definitions. The study of the overlap between P13 and AH13 definitions on the Plaschke et al. (2013) survey showed agreement only in 17% of the events (Vuorinen et al., 2019). The authors suggested that the AH13 criterion includes not only jets but the numbers of the other structures close to the magnetopause.

The criterion used in this work is a combination of the AH13 and P13 criteria. According to this, a jet event is a time interval where P_{dx} is greater than $0.4 \cdot P_{\mathrm{dsw}}$ for all measurement points and the maximum P_{dx} in this interval is greater than P_{dsw}. As a result, 1,400 jets are selected based on these criteria. According to AH13, jets are only considered when the maximum dynamic pressure (P_{d}) of the jet is greater than twice the 20-min temporal average of the surrounding magnetosheath dynamic pressure. Our selected events show excellent agreement with this criterion.

Localized structures with an electron density of at least 50% higher than the surrounding plasma were termed as plasmoids by Karlsson et al. (2012). According to Gunell et al. (2012, 2014), plasmoids are associated with an increase in flow velocity. Plasmoids with velocity changes of more than 10% were termed fast plasmoids by Karlsson et al. (2012, 2015). Only half of the selected events in our study fully meet this criterion. In the present paper, we refer them as "fast plasmoids."

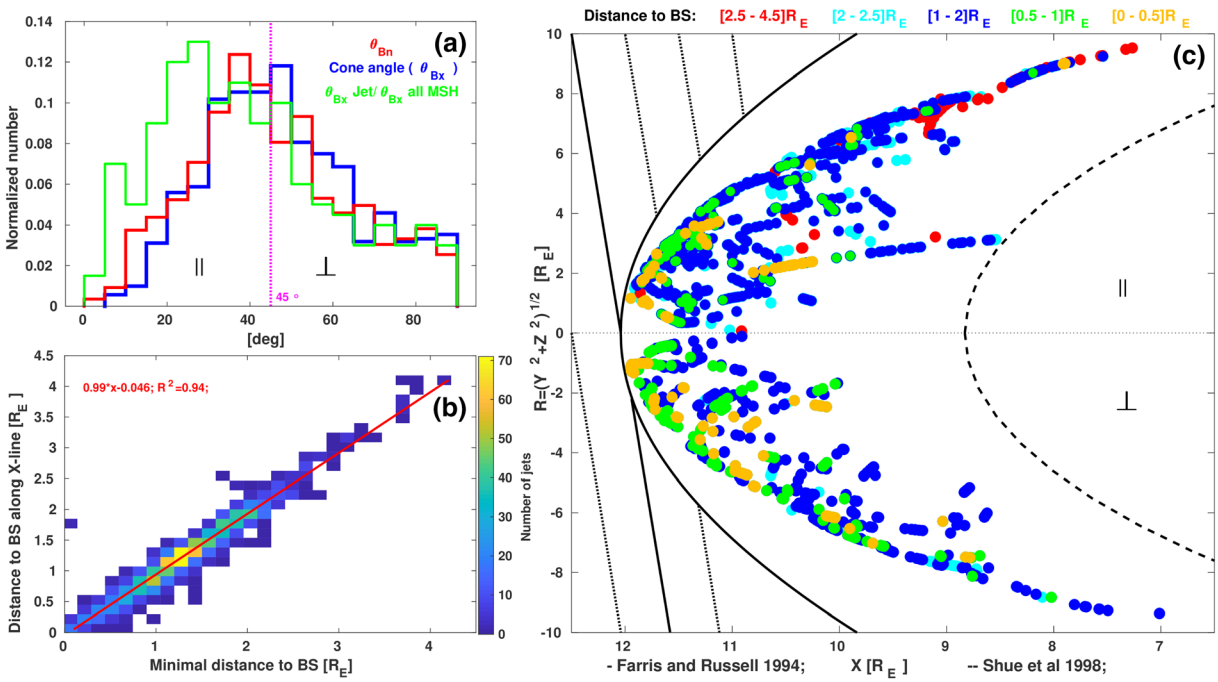

Figure 1. (a) Distributions of the local θ_{Bn} and cone angles ($\theta_{Bx} = \cos^{-1}(B_x/|B|)$) during jet observations are represented by red and blue colored lines, respectively. The green line represents jet occurrence probability as a ratio of the cone angle distributions: during jet observation (θ_{Bx} *Jet*) and during the magnetosheath intervals (θ_{Bx} all *MSH*). (b) The number of jets (color coded) as a function of the distance along *X* line and the minimal distance to the bow shock in GSE coordinate system. (c) Map of jets in the quasi-parallel ($R > 0$) and quasi-perpendicular magnetosheath ($R < 0$) in the XR_{GSE} plane. Parabolas indicate modeled position of bow shock (Farris & Russell, 1994) and magnetopause (Shue et al., 1998). Color coding corresponds to distance to the bow shock.

The upstream solar wind parameters (i.e., magnetic field, velocity, density, and temperature) were obtained from the 1-min OMNI solar wind data, propagated to the bow shock nose and consisted of measurements from different spacecraft around the L1 point. For instance, to compensate the uncertainty of the solar wind propagation from the spacecraft at the L1 point to the bow shock as well as to the jet locations, all upstream solar wind parameters were calculated by averaging the data 4 min before and after the observations of jets. To obtain the minimal distance between the bow shock and the spacecraft as well as the local bow shock normal, the calculated solar wind parameters were compared with the Farris and Russell (1994) bow shock model.

3. Observations

Early studies of jets in the magnetosheath have indicated that the jet formation is closely related to processes in the foreshock region of quasi-parallel bow shock. Our data set shows that jet occurrence downstream of the quasi-perpendicular shock is not uncommon. However, one should note that we have used a somewhat different selection criterion, and the jets in our data set show higher antisunward velocity enhancements. Figure 1a presents the distributions of the θ_{Bn} and cone angles at time of jet observations, represented by red and blue colored lines, respectively. Figure 1a shows that such jets are observed in a wide range of θ_{Bn} and cone angles but are primarily observed during typical Parker's spiral IMF (i.e., cone angles ~45°). However, the normalized distribution of cone angles (green line) shows that jets occur much more often downstream of the quasi-parallel bow shock.

The θ_{Bn} angle calculated at the closer bow shock point provides actual information about the magnetosheath, where jet propagated. According to previous studies, the velocity of magnetosheath jets is generally oriented more along the Sun-Earth line (Archer & Horbury, 2013; Gunell et al., 2012; Hietala et al., 2012; Hietala & Plaschke, 2013; Plaschke et al., 2013). Figure 1b presents the relationship between the distance along the Sun-Earth line and the minimal distance to the bow shock in geocentric solar ecliptic (GSE) coordinate system. Due to the orbits of the MMS spacecraft during 2015–2017, the magnetosheath intervals are

mainly observed in the subsolar magnetosheath, and the differences between these distances are small. However, jets are connected not only with the increasing of the X component of the velocity flow. The values of the Y and/or Z components can be up to 70% of X, and they can affect the jet propagation direction. For this reason, in our analysis, we use the minimal distance to follow the jet propagation.

On the other hand, the θ_{Bn} angle highly affects the propagation of the jets. Figure 1c presents a map of the jet location in XR_{GSE} plane, where $R_{GSE} = \sqrt{Y_{GSE}^2 + Z_{GSE}^2}$ in the GSE coordinate system. In this figure, the locations of the jets are separated based on whether they are observed in the regions of quasi-parallel or quasi-perpendicular magnetosheath. Jets that are observed downstream of quasi-parallel (quasi-perpendicular) shock are plotted in the positive (negative) R_{GSE} region. The colored dots correspond to different ranges of the minimal distance from the jets to the model bow shock locations. It is seen in Figures 1b and 1c that jets can be observed in a wide range of distance to the bow shock, but they are predominantly found closer to the bow shock (distance from the bow shock <2 R_E) than to the magnetopause. A similar result was also noted by Plaschke et al. (2013). However, it is noteworthy to mention that jets downstream of the quasi-perpendicular shock are observed only up to 2.5 R_E. Palmroth et al. (2018) used a global hybrid simulation and found that the jet dynamic pressure is greatest nearest to the shock and decreases as the jets propagate toward the magnetopause. The dynamic pressure decreases by 70% from the bow shock to the vicinity of the magnetopause. This effect indicates that the origin of the jet may be related to the dynamic pressure upstream the bow shock.

Our statistical analysis is based on MMS observations in the magnetosheath. One thousand four hundred jets were selected in this work, and as shown in Figure 1b, about 35% of the events were observed downstream of the quasi-perpendicular bow shock. One example of such events is shown in Figure 2. On 25 October 2015, the MMS spacecraft were located at [10.05; 6.47; −0.67] R_E. OMNI cone angle is shown in Figure 2a, and the magnetosheath parameters (i.e., plasma velocity along the Earth-Sun line, ion energy-time spectrogram of energy flux, and dynamic pressure) from MMS1 spacecraft in fast mode are shown in Figures 2b to 2d. The cone angle of the entire interval shown in Figure 2a is always greater than 50°, suggesting that the spacecraft is located downstream of the quasi-perpendicular bow shock. In addition, the rather narrow ion energy range shown in Figure 2c is a typical characteristic of the quasi-perpendicular magnetosheath. Furthermore, according to the Farris and Russell (1994) bow shock model, the spacecraft were located approximately 0.85 R_E from the bow shock, with local bow shock normal $\boldsymbol{n} = [0.95; 0.23; -0.16]$ and $\theta_{Bn} = 70°$.

At around 10:18 UT (the red-boxed region in Figures 2a to 2d), three jets with rapid increases/enhancements in the X-component of plasma velocity and the total dynamic pressure were identified (i.e., Figures 2b and 2d). The high time resolution plasma measurements (burst mode) of this interval are expanded and presented in Figures 2e to 2l. Due to the close MMS spacecraft configuration on this particular date which are in the order of a few tens of kilometers (i.e., much smaller than the typical scale sizes of jets), measurements of all spacecraft are almost the same (see Figures 2h and 2k). Hence, only data from MMS1 are shown here.

As previously noted, the number of jets identified is highly sensitive to the selection criteria. The application of a different selection criterion over the same time interval as shown in Figures 2e to 2l could result in a different number of jets. For instance, the AH13 criterion would have identified the five jets which are marked by the blue and yellow dashed lines in Figures 2e to 2l. On the other hand, the initial P13 criterion would have identified four of these jets, and three of them (marked by blue dashed lines) matched the identified jets in this work. On the contrary, only two (marked by yellow dashed lines) of these five jets would have been identified if the K12 selection criterion had been applied instead. The different discussed criteria are reflected in Figures 2k and 2l.

In a case study, Eriksson et al. (2016) observed a high current density inside a jet and concluded that a current sheet had formed at the boundary between colder, more solar wind-like plasma and warmer, magnetosheath-like plasma. The current sheet, as well as the jet, propagated from the bow shock toward the magnetopause. Detailed analysis of jet by Plaschke et al. (2017) showed that jet can have a significant substructure, including the current sheet and waves. Similar to previously reported jets which predominantly have been observed in the quasi-parallel magnetosheath (e.g., Eriksson et al., 2016; Plaschke et al., 2013, 2017), the jets we identify in this work, downstream of quasi-perpendicular shock, are also

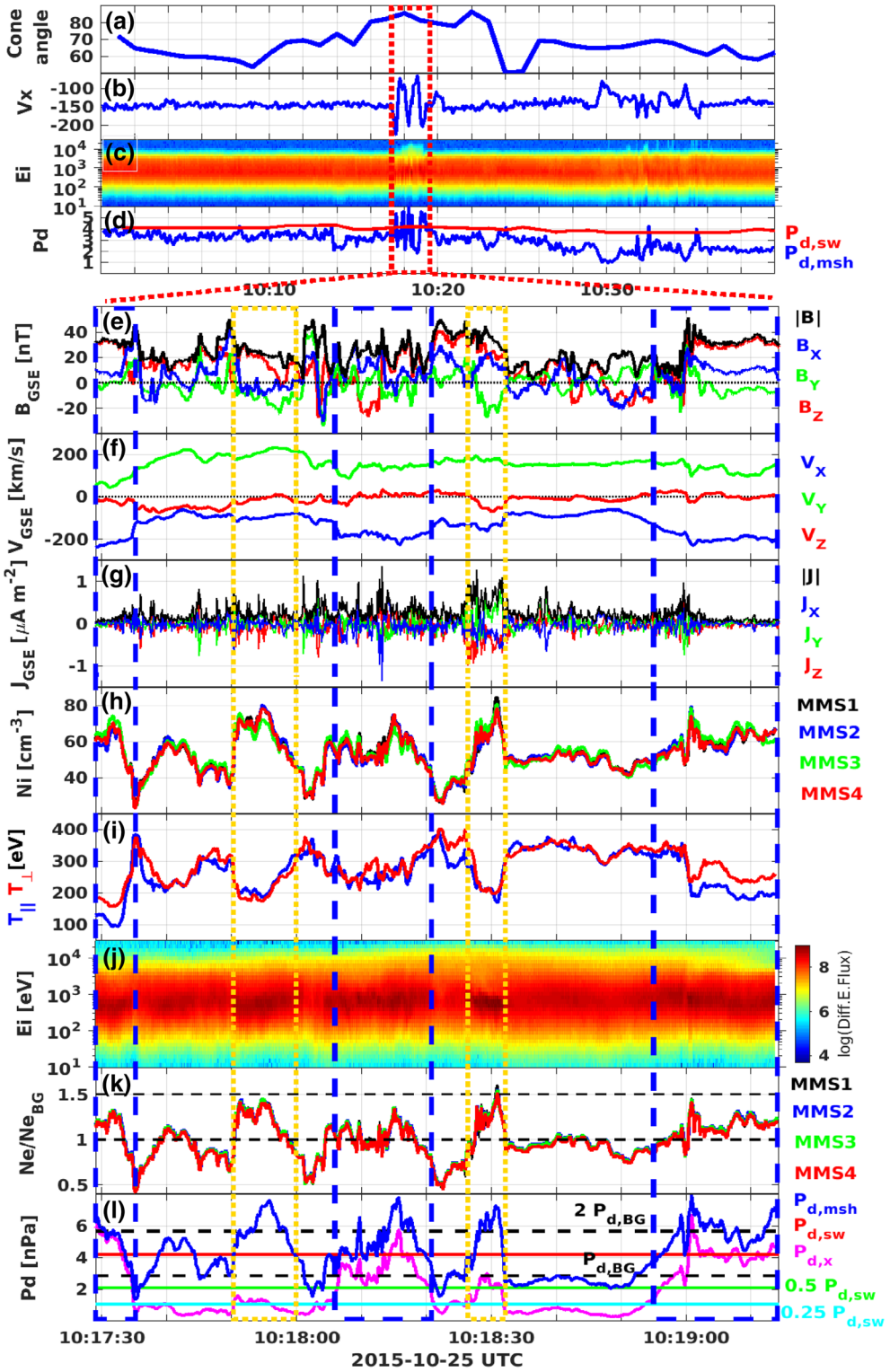

Figure 2. The orientation of the IMF with respect to the Earth-Sun line propagated to the nose of bow shock (a) and (b–d) MMS1 observations in the magnetosheath on 25 October 2015. (e–l) Enlarged intervals of the box with red dashed lines showing a series of the jets in the x-component of velocity. The ion density (h) and electron density ratio (k) are shown from all four spacecraft. The last two panels indicated the identification criteria of (k) K12 (yellow boxes), (l) AH13 (both yellow and blue boxes), and (l) P13 (blue boxes). See the main text for descriptions of each method.

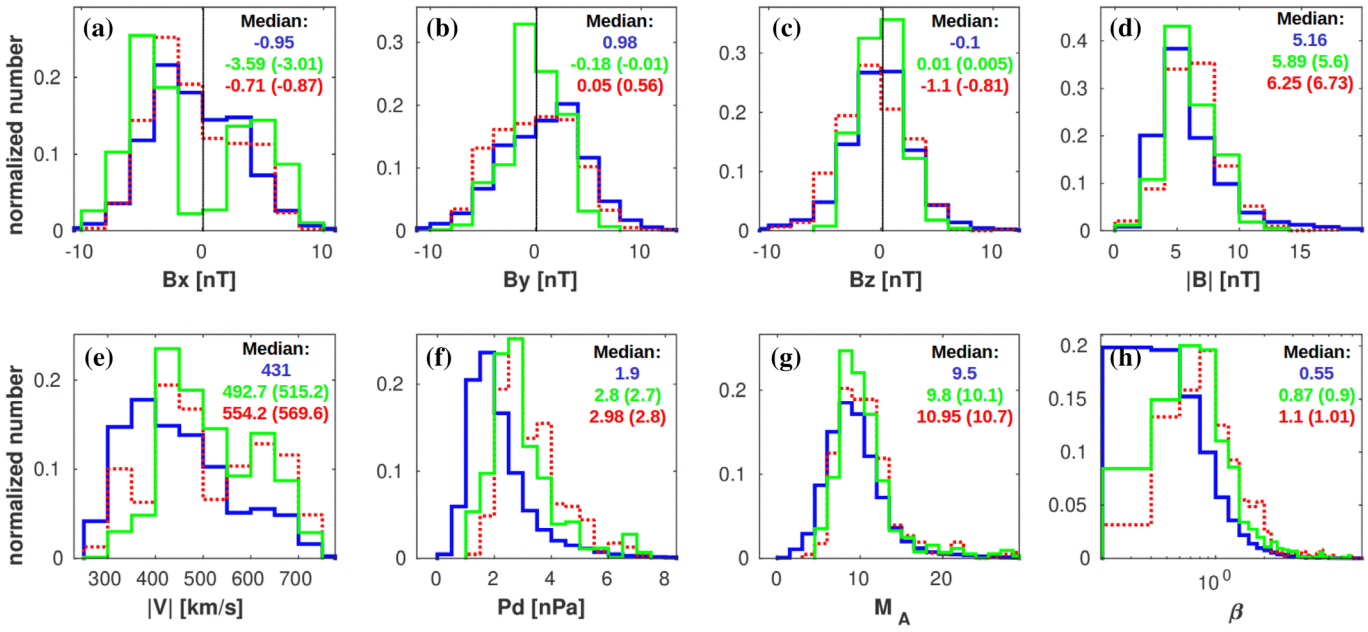

Figure 3. Distributions of the upstream solar wind parameters during October 2015 to January 2016 and October 2016 to February 2017. (a–c) *XYZ* components of the IMF; (d) total solar wind magnetic field; (e) total velocity of the solar wind; (f) total solar wind dynamic pressure; (g) Alfvén Mach number; and (h) plasma beta. The values in brackets correspond to fast plasmoids, and colors represent jets in the quasi-parallel (green) and quasi-perpendicular (red) magnetosheath. The blue lines show the distribution for the whole observational interval, that is to say, both inside and outside the jets.

associated with current density enhancements (Figure 2g). In Figure 2j, it is seen that the ion energy flux is high inside the jets, peaking at an energy of ~0.8 keV, which is not far below the typical solar wind proton energy of ~1 keV. However, these signatures can also be observed for "small jets" that do not match any of the criteria discussed in this work, for example, in the approximate period from 10:17:36 to 10:17:46 UT as shown in Figure 2j. Hence, jets should not be identified based solely on one single parameter. A comparison of the energy flux with signatures in other measured quantities is more likely to provide a good identification criterion.

Based on the magnetic field strength compared to the surrounding background field, Karlsson et al. (2015) divided the plasmoids they observed into two distinct groups. Plasmoids that were associated with clear magnetic field increases were called "paramagnetic," and plasmoids with clear decreases were called "diamagnetic." The majority of the jets and fast plasmoids identified in our data set have paramagnetic signatures. However, it is of interest to note that the magnetic field signatures within the jets and fast plasmoids themselves are not always same. For instance, it is shown in Figure 2e that the magnetic field of the jets (boxes with blue dashed lines) are accompanied with larger fluctuations and more rapid rotations compared to the fast plasmoids (boxes with yellow dashed lines). However, a more detailed analysis with a larger number of examples is needed and will be done in the near future.

On the other hand, the changes in the ion and electron densities of the jets and plasmoids show excellent anticorrelation with the changes in ion temperature (comparing Figures 2h and 2k to Figure 2i). Such a signature is observed in all 1,400 cases (results not shown) and is consistent with the study by Gutynska et al. (2015), who analyzed jets based on density enhancements using a K12 criterion. An anticorrelation between density and temperature is a typical signature of magnetosonic waves. In other words, these results suggest that jets and fast plasmoids are magnetosonic in nature.

4. Upstream and Downstream Conditions

Apart from the clear dependence on cone angles, Plaschke et al. (2013) pointed out that jets in the quasi-parallel magnetosheath have rather weak to insignificant dependence on solar wind velocities and magnetic field strengths. Figure 3 shows histograms of the upstream solar wind parameters, (a-d)

magnetic field components and magnitude, (e) plasma velocity magnitude, (f) dynamic pressure, (g) Alfvén Mach number ($M_A = |V|/V_a$, where $V_a = |B|/\sqrt{\mu_0 \rho}$ is the Alfvén speed and μ_0 the vacuum permittivity), and (h) plasma beta ($\beta = 2\mu_0 k_B NT/|B|^2$, where k_B is Boltzmann's constant, N is the solar wind density, and T is the solar wind temperature), at the time when the jets were observed in quasi-parallel (green lines) and quasi-perpendicular (red lines) magnetosheath. In all panels, the blue lines show the respective parameters in the entire time periods regardless of whether jets were identified. Figures 3a to 3c show that there is no (clear) dependence between the jet occurrence and the IMF orientations. In Figures 3d and 3e, the difference between the blue and green distributions shows that the occurrence of jets in the quasi-parallel magnetosheath has clearer dependence on the magnitude of both the magnetic field and plasma velocity. In addition, our results show that the occurrence of jets in the quasi-perpendicular magnetosheath is linked to higher (about 20%) solar wind magnetic field and plasma velocity magnitudes than jets in the parallel magnetosheath. Similar dependence can also be observed in the dynamic pressure and Alfvén Mach number shown in Figures 3f and 3g. Furthermore, in contrast to Plaschke et al. (2013), the occurrence of jets in our work shows strong dependence on the solar wind plasma beta. In particular, higher plasma beta is observed when jets are present in the magnetosheath. The plasma beta is 30% higher when the jets are observed in the quasi-perpendicular magnetosheath compared to quasi-parallel magnetosheath (red and green lines in Figure 3h).

Figure 4 shows the change in direction of the magnetic field and the plasma bulk velocity between the solar wind, the magnetosheath, and the jets. Figure 4a shows a histogram of the angle between the velocity vector in the solar wind and in the magnetosheath, and Figure 4b shows how this angle varies with the distance to the bow shock. Histograms of the angle between the magnetic field in the solar wind and in the magnetosheath and how it changes with the distance to the bow shock are shown in Figures 4c and 4d, respectively. In all panels, the quasi-parallel magnetosheath is shown in green and the quasi-perpendicular in red. The 95% confidence intervals of the medians are shown by colored dotted lines in the first and fourth columns and by colored area in the second and third columns. The changes of the IMF orientation in the quasi-perpendicular magnetosheath are smaller (red line in Figure 4d) than in the quasi-parallel magnetosheath. Dimmock and Nykyri (2013) showed that the quasi-perpendicular magnetosheath is a region favorable to magnetic field and velocity asymmetry (i.e., velocity and magnetic field strength are larger on the dusk flank) during typical Parker spiral IMF conditions. However, deflections of the plasma flow in the quasi-parallel and quasi-perpendicular magnetosheaths are almost the same (Figure 4a). The triangles and circles in Figures 4b and 4c show that the deflection of the IMF and plasma flow from the solar wind orientation increases with the propagation depth in the sheath. Due to higher fluctuations in the quasi-parallel magnetosheath, calculation errors of the magnetic field rotation are rather large (green triangles).

Previous studies concluded that the velocity of magnetosheath jets is generally oriented more along the Sun-Earth line (Archer & Horbury, 2013; Gunell et al., 2012; Hietala et al., 2012; Hietala & Plaschke, 2013; Plaschke et al., 2013). We find that the median deflection of the solar wind flow from the Sun-Earth line is 2.68° (not shown). Figures 4e to 4h show the changes of the jet plasma flows, as well as the magnetic fields, from the solar wind orientation. The colored circles in Figure 4f show that the deflection angle increases with bow shock distance, similar to the magnetosheath plasma in Figure 4b. However, the jets are not deflected as much as the rest of the magnetosheath. For instance, the deflection angle between the jet and the magnetosheath plasma is about 15°, as shown in Figure 4i. Gunell et al. (2012) concluded that the plasmoids move predominantly in a tangential direction with respect to the magnetopause normal. On the other hand, Hietala and Plaschke (2013) reported that the jets have a tendency to continue "straight" along the Sun-Earth line as compared to the background magnetosheath flow. The deflection from the background magnetosheath flow is in the range of 20° to 45°. Plaschke et al. (2013) reported a number of 28.6° for the median deflection. In our statistics, the median deflection for both types of jets are quite similar and in a good agreement with the early reported range (Figures 4i to 4l). Thus, we conclude that the direction of propagation is in between the extremes of being tangential to the magnetopause and continuing straight in the solar wind direction. Figures 4j to 4k show that differences of the magnetic field (triangles) and flow (circles) orientations inside and outside of the jet slightly decreases with propagation depth in the quasi-parallel magnetosheath. Nevertheless, in the quasi-perpendicular magnetosheath, the deflection angle is almost constant with the propagation depth, and this confirms the hypothesis that the jets move in their original direction with respect to the magnetosheath.

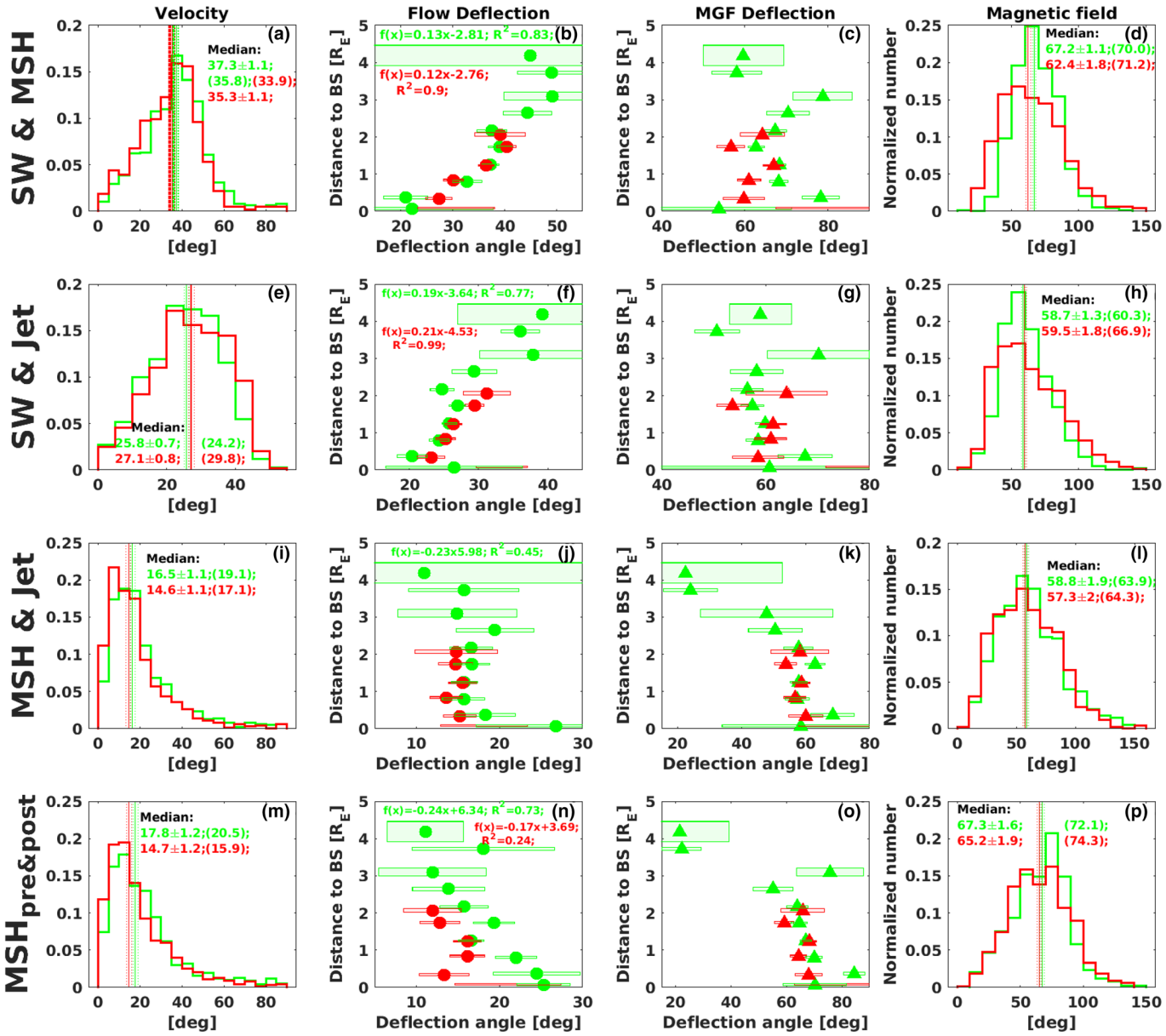

Figure 4. Histograms of the plasma flow (left column) and magnetic field (right column) deflections in the quasi-parallel (green) and quasi-perpendicular (red) magnetosheath. Changes of the deflection angles with the distances to bow shock are shown in the two central columns. The panels (a)–(d) and (e)–(h) presents changes of the solar wind parameters in the magnetosheath (SW&MSH) and inside jet (SW&Jet). Differences of the magnetosheath parameters inside (MSH&Jet) and around ($MSH_{pre\&post}$) jets are presented in panels (i)–(l) and (m)–(p), respectively. In all panels, the green and red colors represent the quasi-parallel and the quasi-perpendicular magnetosheath, respectively. Filled circles correspond to velocity deflections and filled triangles to magnetic field deflections. The 95% confidence intervals of the medians are shown by colored dotted lines in the first and fourth columns and by colored area in the second and third columns.

Propagating through the magnetosheath, jets do not only affect the magnetopause and magnetosphere. Simulation results by Karimabadi et al. (2014) showed that jets pushed slower ambient magnetosheath plasma out of their way. As a result, the plasma moves around the jets, and it is slowed down or could even be pushed in the sunward direction. Consequently, jets may create anomalous flows and be a source of additional turbulence. Figure 4m shows a histogram of the angle between the magnetosheath flow direction ahead and behind the jets. In this work, the majority of the jets are associated with small changes in the magnetosheath flow. However, from Figure 4p, it can be seen that jets are accompanied by strong changes in the

magnetosheath magnetic field orientation. On the other hand, the influence of the jets on the surrounding magnetosheath decreases with the propagation distances (Figures 4n and 4o).

The magnetosheath jet velocity is considerably greater than the local Alfvén velocity. Some jets are also supermagnetosonic and may even be associated with a local shock at the front of the jet (Hietala et al., 2009, 2012; Plaschke et al., 2017; Plaschke & Hietala, 2018). In our analysis, about 95% of jets are superalfvénic (not shown) with median Alfvénic Mach number of 1.8 in the quasi-parallel and 1.6 in the quasi-perpendicular magnetosheath. Nevertheless, only 12% of them are supermagnetosonic (i.e., jet speed is higher than magnetosonic speed, $V_{\mathrm{ms}} = \sqrt{V_A^2 + C_S^2}$, where $C_s = \sqrt{\gamma k_B (T_e + T_i)/(m_i + m_e)}$ is the sound speed, γ is the adiabatic index). Plaschke et al. (2013) noted that in the subsolar region, only about 14% of jets are supermagnetosonic. Archer and Horbury (2013) suggested that the majority of the supermagnetosonic jets must be observed in the flanks of the magnetosheath. On the other hand, they pointed out that density-driven jets are more likely to occur at the flanks. The global electromagnetic hybrid simulations of the structures with density enhancements by Omidi et al. (2014) predicted their propagation into the magnetosheath at the flanks. The small apogee of the MMS orbit during the entire period do not allow a clear conclusion about jets at the flanks. Further analysis of the MMS measurements at the magnetosheath flanks on 2017–2018 is necessary and should be done in the near future.

Covering the whole dayside region, Archer and Horbury (2013) reported that there is no clear change in observation probability with distance from the bow shock. The analysis of plasmoids in the magnetosheath by Karlsson et al. (2015) showed that plasmoids with changes in velocity are found for $X_{\mathrm{GSE}} > 2\ R_{\mathrm{E}}$, while plasmoids without velocity changes (labeled embedded plasmoids by Karlsson et al., 2015) are found further downstream for $X_{\mathrm{GSE}} > -5\ R_{\mathrm{E}}$. Figures 1b, 1c, 4f, and 4j show that velocity-driven jets are more common close to the bow shock and deflections from the magnetosheath flow decrease with increasing propagation distances. Such an effect can be the result of jets slowing down while propagating through the magnetosheath. Figure 5 shows the ratio of jet speed to magnetosheath flow speed as a function of bow shock distances for jets (a, b) and fast plasmoids (c, d) in the quasi-parallel and quasi-perpendicular magnetosheaths. In the quasi-parallel magnetosheath as well as in the quasi-perpendicular, the median values in each 0.5 R_{E} distance bins show a signature of the jets and fast plasmoids slowing down. Similar signatures were observed by Dmitriev and Suvorova (2015), who followed jets with the five THEMIS spacecraft and reported a decrease of the jet velocity as it moved toward the magnetopause. Differences of the deceleration trend in the quasi-perpendicular and quasi-parallel magnetosheath can be connected with the formation mechanisms and the asymmetry of the magnetosheath magnetic field and velocity, associated with a quasi-perpendicular bow shock (Dimmock & Nykyri, 2013).

5. Discussion

We have presented a statistical study of magnetosheath jets and fast plasmoids in the quasi-parallel and quasi-perpendicular magnetosheaths. We compared the main observational criteria used in the past (Archer & Horbury, 2013; Karlsson et al., 2012, 2015; Plaschke et al., 2013), and we could verify the properties of jets and fast plasmoids. Our results mainly confirmed previous statistical studies and show good agreement between jets and fast plasmoids. We showed that jets occur not only downstream of the quasi-parallel shock and that jets in the quasi-perpendicular magnetosheath are not rare. We found that the occurrence of jets is not exclusive to low IMF cone angles and they can be detected even during a perpendicular IMF orientation. The existence of jets in the quasi-perpendicular magnetosheath is mainly connected with oblique IMF orientations. A strong solar wind with higher than average velocity and magnetic field (i.e., higher Alfvén Mach number and plasma beta) creates conditions favorable for the generation of jets.

As they propagate through the magnetosheath, the jets accelerate slower plasma ahead of them in their propagation path and push it out of their way (Plaschke & Hietala, 2018), and they are slowed down in the process. Dmitriev and Suvorova (2015) discussed a large-scale jet whose velocity decreased about 20% over a 1.4 R_{E} propagation distance in the magnetosheath. The trends in Figure 5 show a quite fast deceleration rate in both the perpendicular and parallel magnetosheath. According to the best fit equation in our results, at distances of about 10–11 R_{E} from the bow shock, jets will have acquired the same velocity as the surrounding magnetosheath. The jets and fast plasmoids in the quasi-perpendicular magnetosheath have shown much

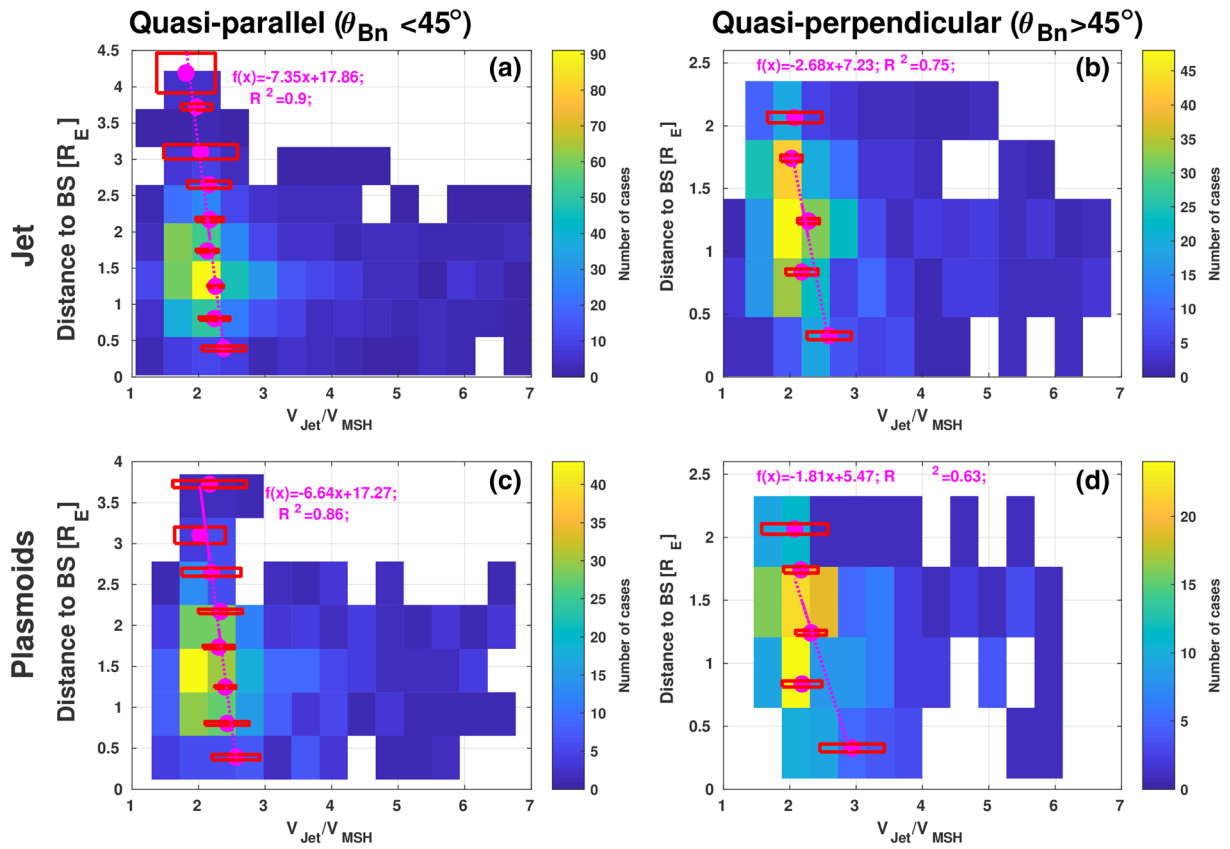

Figure 5. Changes of the flow velocities inside jets (a, b) and fast plasmoids (c, d) regarding the local speed with bow shock distances in the quasi-parallel (left) and quasi-perpendicular (right) magnetosheath. The median values of jets (a, b) and fast plasmoids (c, d) in each 0.5 R_E bin and their 95% confidence intervals are marked by red dots and lines, respectively.

faster deceleration and at distances of about 4–5 R_E will be embedded in the magnetosheath flow. Such fast deceleration of jets and plasmoids in the magnetosheath can explain the results of Karlsson et al. (2015), who pointed out that plasmoids were observed up to $X_{GSE} = -5\ R_E$, but fast plasmoids only until $X_{GSE} = 2\ R_E$. Figures 4j and 5a indicate that the propagation of jet through the magnetosheath since their formation is not constant. This may provide hints on their propagation evolution. It is clear seen that tangential flows are significant and not negligible. Hence, it remains a question whether the jets in their later stages (deeper in the magnetosheath when they may have lost their initial propagation momentum) would still propagate mainly in their nominal directions or flow along the now-ambient sheath flow. Further work should be done to validate this hypothesis.

What mechanism leads to the formation of jets is still under debate. Many different models have been suggested. The majority of these conclude that foreshock processes are responsible for generating most of the jets (Hietala et al., 2012; Hietala & Plaschke, 2013; Plaschke et al., 2013). Among the more notable of the suggested mechanisms, we find *bow shock ripples* and *SLAMS*, which are both inherent to the quasi-parallel shock, although ripples have also been observed on the quasi-perpendicular shock (Johlander et al., 2016, 2018). On the other hand, Archer et al. (2012) suggested that jets could form when the shock locally changes from quasi-parallel to quasi-perpendicular or vice versa due to IMF discontinuities passing the bow shock. However, jets are mostly observed during steady IMF, and only 15% of the jets in this study were connected with a clear signature of a solar wind discontinuity. For this reason, alternative formation mechanisms are also needed to explain the observations.

Early estimates of the size of the magnetosheath jets gave values in the order of 1 R_E (Archer et al., 2012; Gutynska et al., 2015; Hietala et al., 2009, 2012; Karlsson et al., 2012, 2015). However, reports of the detailed morphology of the jets have been somewhat inconsistent. Archer et al. (2012) report a longer scale size parallel to the jet flow than perpendicular to it. Plaschke et al. (2016) interpreted their results as the jets having a

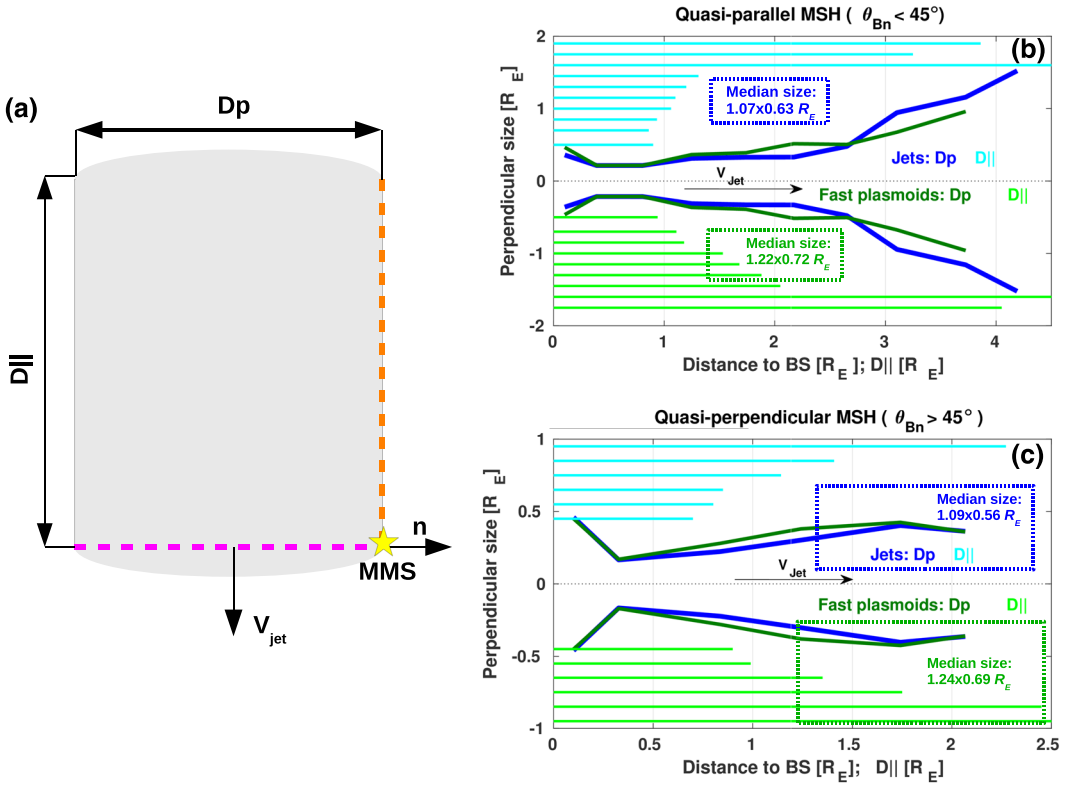

Figure 6. Conceptual figures of the jet morphology (a). The assumed position of the spacecraft is shown by a yellow five-pointed star. The orange dashed line shows the trajectory of the jet crossing when it moves parallel to the plasma flow. The trajectory of the cross scale size estimation is represented by a magenta dashed line. Changes of the jets and fast plasmoids shapes in the quasi-parallel (b) and quasi-perpendicular magnetosheaths (c). The blue (light blue) and green (light green) lines represent cross scale (parallel to the plasma flow) sizes of the jets and fast plasmoids, respectively. The parallel size of the jets and plasmoids is almost two times higher than perpendicular size in both the parallel and perpendicular magnetosheath. The median shapes are shown as dotted color rectangles.

pancake-like geometry. Similar to previous studies, we assumed a cylindrical jet geometry. The dimension along the flow direction ($D||$) was estimated for every jet and fast plasmoid observation by integrating the ion velocity over the jet duration (Δt). The duration times were determined as the time of jet observation, where the P_{dx} is greater than $0.4 \cdot P_{dsw}$. An upper limit of the flow parallel size was proposed by Gunell et al. (2014) as the product of the duration and maximum speed, and this provide excellent agreement with $D||$ in the all distance ranges (not shown).

To determine thickness (Dp) of jets, we use the Rankine-Hugoniot relations (Koval & Szabo, 2008) to obtain the local normal and speed along this estimated normal. In particular, we require the angle between the obtained normal and the jet flow direction to be in the 80° to 100° range. Applying these criteria, we obtain a set of 980 cases of jet and fast plasmoid observations in the quasi-parallel and quasi-perpendicular magnetosheaths. Assuming that the jet propagated along the normal with the estimated speed, the jet thickness was calculated. The thickness is an overestimate as we have not taken into account propagation parallel to the flow (V_{jet}). Figure 6a shows a sketch of our assumption. The spacecraft is located on top, and the estimated trajectory of its motion is shown by dashed colored lines. Figures 6b and 6c show the shapes of the jets (blue) and fast plasmoids (green) in the quasi-parallel (b) and quasi-perpendicular (c) magnetosheaths. The light blue and light green lines, in both figures, represent the median values of the jet and fast plasmoid $D||$ sizes at different distances from the bow shock. The dotted rectangles in panels (b) and (c) represent the median size of the jets (blue) and fast plasmoids (green) in both types of the magnetosheath.

Figure 7 shows how the parallel (a, b) and perpendicular (c, d) scale sizes change with the distance from bow shock. The median values in each 0.5 R_E bin and their 95% confidence intervals are shown by red circles and

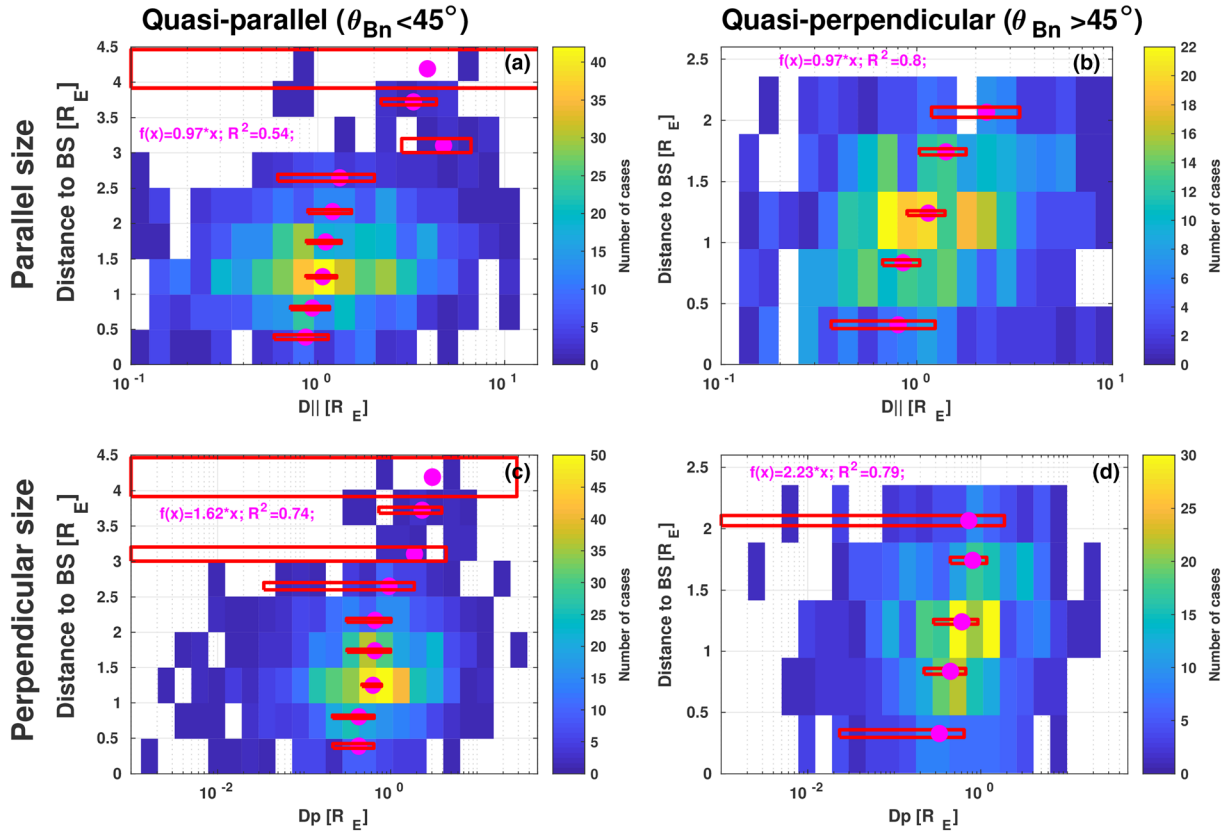

Figure 7. Diagrams of jet observations in a size-distance plane. The top panels (a, b) show the length parallel to the direction of propagation, and the lower panels (c, d) show the jet extent in the dimension perpendicular to the direction of propagation. The left and right columns represent observations in the quasi-parallel and quasi-perpendicular magnetosheaths, respectively. The large filled red circles show median values in each 0.5 R_E bin, and red lines represent their 95% confidence intervals.

dotted rectangles, respectively. All plots indicate continuous increasing trends of the parallel, $D||$ (upper panels), and perpendicular, Dp (lower panels), dimensions of jets in the quasi-parallel (left) and quasi-perpendicular (right) magnetosheath. The median values show that the extent of both jets and fast plasmoids parallel to the direction of propagation is almost twice as high as the perpendicular extent irrespective of magnetosheath type. A similar conclusion was reported by Archer et al. (2012). However, the slopes of the curves described by the red circles indicate that the jets expand faster in the perpendicular than the parallel direction as they travel through the magnetosheath. Similar results were observed for fast plasmoids (not shown) and confirmed the conclusion by Karlsson et al. (2015) that the plasmoids are a subset of magnetosheath jets.

6. Summary and Conclusion

Based on our analysis of 1,400 events, with higher enhancements in the X component of the velocity, in a broad range of the magnetosheath and upstream parameters, we can summarize our conclusions in the following list.

1. The basic properties of jets and fast plasmoids are very similar.
2. The probability of jet generation increases when the solar wind is stronger, that is, when it has a higher velocity, magnetic field, Alfvén Mach number, and plasma beta.
3. Jet observations in the quasi-perpendicular magnetosheath are relatively common.
4. Jet observations are more frequent close to the bow shock, and their direction is toward the magnetopause.
5. A low θ_{Bn} angle enables propagation deeper into the magnetosheath.

6. The propagation speed of a jet decreases as it moves toward the magnetopause, and during its propagation, the velocity of the jet tends toward the velocity of the surrounding magnetosheath.
7. The typical size of these structures is several thousands of kilometers, and it increases with the distance to bow shock.
8. The parallel size of the jets and plasmoids is almost two times higher than perpendicular size in both the parallel and perpendicular magnetosheaths.

Our comparative analysis showed no significant differences between the plasma properties of the jets and fast plasmoids. However, the different magnetic fields inside the structures suggest that the formation mechanisms are different. Palmroth et al. (2018) found that the criteria applied by Archer and Horbury (2013) and Karlsson et al. (2012) provide a better opportunity than the criterion by Plaschke et al. (2013) to detect jets "shaped more like blobs." Further comparative analysis of the detailed structure of these plasmoids and jets is necessary and will be conducted in the near future.

Data Availability Statement

All data are available through https://omniweb.gsfc.nasa.gov/ and https://lasp.colorado.edu/mms/sdc/public/.

Acknowledgments
O.G. was supported by the Kempe Foundation, H.G. by the Belgian Science Policy Office through the Solar Terrestrial Centre of Excellence and by the Swedish National Space Agency (SNSA) Grant 108/18, and M.H. by SNSA. We thank the MMS Science Data Center and all the MMS teams, especially the magnetic field and the ion teams, for producing high-quality data. We also acknowledge NASA's National Space Science Data Center and Space Physics Data Facility.

References

Archer, M. O., & Horbury, T. S. (2013). Magnetosheath dynamic pressure enhancements: Occurrence and typical properties. *Annales de Geophysique*, *31*, 319–331. https://doi.org/10.5194/angeo-31-319-2013

Archer, M. O., Horbury, T. S., & Eastwood, J. P. (2012). Magnetosheath pressure pulses: Generation downstream of the bow shock from solar wind discontinuities. *Journal of Geophysical Research*, *117*, 05228. https://doi.org/10.1029/2011JA017468

Blanco-Cano, X., Omidi, N., & Russell, C. T. (2006a). Macrostructure of collisionless bow shocks: 2. ULF waves in the foreshock and magnetosheath. *Journal of Geophysical Research*, *111*, 10205. https://doi.org/10.1029/2005JA011421

Blanco-Cano, X., Omidi, N., & Russell, C. T. (2006b). ULF waves and their influence on bow shock and magnetosheath structures. *Advances in Space Research*, *37*(8), 1522–1531. https://doi.org/10.1016/j.asr.2005.10.043

Burch, J. L., Moore, T. E., Torbert, R. B., & Giles, B. L. (2016). Magnetospheric Multiscale overview and science objectives. *Space Science Reviews*, *199*, 5–21. https://doi.org/10.1007/s11214-015-0164-9

Burgess, D. (1989). On the effect of a tangential discontinuity on ions specularly reflected at an oblique shock. *Journal of Geophysical Research*, *94*(A1), 472–478. https://doi.org/10.1029/JA094iA01p00472

Dimmock, A. P., & Nykyri, K. (2013). The statistical mapping of magnetosheath plasma properties based on THEMIS measurements in the magnetosheath interplanetary medium reference frame. *Journal of Geophysical Research: Space Physics*, *118*, 4963–4976. https://doi.org/10.1002/jgra

Dmitriev, A. V., & Suvorova, A. V. (2015). Large-scale jets in the magnetosheath and plasma penetration across the magnetopause: THEMIS observations. *Journal of Geophysical Research: Space Physics*, *120*, 4423–4437. https://doi.org/10.1002/2014JA020953

Dunlop, M. W., Balogh, A., Glassmeier, K.-H., & Robert, P. (2002). Four-point Cluster application of magnetic field analysis tools: The Curlometer. *Journal of Geophysical Research*, *107*(A11), 1384. https://doi.org/10.1029/2001JA005088

Eriksson, E., Vaivads, A., Graham, D. B., Khotyaintsev, Y. V., Yordanova, E., Hietala, H., et al. (2016). Strong current sheet at a magnetosheath jet: Kinetic structure and electron acceleration. *Journal of Geophysical Research: Space Physics*, *121*, 9608–9618. https://doi.org/10.1002/2016JA023146

Farris, M. H., & Russell, C. T. (1994). Determining the standoff distance of the bow shock: Mach number dependence and use of models. *Journal of Geophysical Research*, *99*(A9), 17681. https://doi.org/10.1029/94JA01020

Goncharov, O., Safrankova, J., Nemecek, Z., Prech, L., Pitna, A., & Zastenker, G. N. (2014). Upstream and downstream wave packets associated with low-Mach number interplanetary shocks. *Geophysical Research Letters*, *41*, 8100–8106. https://doi.org/10.1002/2014GL062149

Gunell, H., Nilsson, H., Stenberg, G., Hamrin, M., Karlsson, T., Maggiolo, R., et al. (2012). Plasma penetration of the dayside magnetopause. *Physics of Plasmas*, *19*(7), 072906. https://doi.org/10.1063/1.4739446

Gunell, H., Stenberg Wieser, G., Mella, M., Maggiolo, R., Nilsson, H., Darrouzet, F., et al. (2014). Waves in high-speed plasmoids in the magnetosheath and at the magnetopause. *Annales de Geophysique*, *32*, 991–1009. https://doi.org/10.5194/angeo-32-991-2014

Gutynska, O., Sibeck, D. G., & Omidi, N. (2015). Magnetosheath plasma structures and their relation to foreshock processes. *Journal of Geophysical Research: Space Physics*, *120*, 7687–7697. https://doi.org/10.1002/2014JA020880

Hietala, H., Laitinen, T. V., Andréeová, K., Vainio, R., Vaivads, A., Palmroth, M., et al. (2009). Supermagnetosonic jets behind a collisionless quasiparallel shock. *Physical Review Letters*, *103*, 245001. https://doi.org/10.1103/PhysRevLett.103.245001

Hietala, H., Partamies, N., Laitinen, T. V., Clausen, L. B. N., Facskó, G., Vaivads, A., et al. (2012). Supermagnetosonic subsolar magnetosheath jets and their effects: From the solar wind to the ionospheric convection. *Annales de Geophysique*, *30*(1), 33–48. https://doi.org/10.5194/angeo-30-33-2012

Hietala, H., & Plaschke, F. (2013). On the generation of magnetosheath high-speed jets by bow shock ripples. *Journal of Geophysical Research: Space Physics*, *118*, 7237–7245. https://doi.org/10.1002/2013JA019172

Hoilijoki, S., Palmroth, M., Walsh, B. M., Pfau-Kempf, Y., von Alfthan, S., Ganse, U., et al. (2016). Mirror modes in the Earth's magnetosheath: Results from a global hybrid-Vlasov simulation. *Journal of Geophysical Research: Space Physics*, *121*, 4191–4204. https://doi.org/10.1002/2015JA022026

Johlander, A., Schwartz, S. J., Vaivads, A., Khotyaintsev, Y. V., Gingell, I., Peng, I. B., et al. (2016). Rippled quasiperpendicular shock observed by the Magnetospheric Multiscale spacecraft. *Physical Review Letters*, *117*, 165101. https://doi.org/10.1103/PhysRevLett.117.165101

Johlander, A., Vaivads, A., Khotyaintsev, Y. V., Gingell, I., Schwartz, S. J., Giles, B. L., et al. (2018). Shock ripples observed by the MMS spacecraft: Ion reflection and dispersive properties. *Plasma Physics and Controlled Fusion*, *60*, 125006. https://doi.org/10.1088/1361-6587/aae920

Karimabadi, H., Roytershteyn, V., Vu, H. X., Omelchenko, Y. A., Scudder, J., Daughton, W., et al. (2014). The link between shocks, turbulence, and magnetic reconnection in collisionless plasmas. *Physics of Plasmas*, *21*, 062308. https://doi.org/10.1063/1.4882875

Karlsson, T., Brenning, N., Nilsson, H., Trotignon, J.-G., Vallières, X., & Facsko, G. (2012). Localized density enhancements in the magnetosheath: Three-dimensional morphology and possible importance for impulsive penetration. *Journal of Geophysical Research*, *117*, 03227. https://doi.org/10.1029/2011JA017059

Karlsson, T., Kullen, A., Liljeblad, E., Brenning, N., Nilsson, H., Gunell, H., & Hamrin, M. (2015). On the origin of magnetosheath plasmoids and their relation to magnetosheath jets. *Journal of Geophysical Research: Space Physics*, *120*, 7390–7403. https://doi.org/10.1002/2015JA021487

King, J. H., & Papitashvili, N. E. (2005). Solar wind spatial scales in and comparisons of hourly wind and ACE plasma and magnetic field data. *Journal of Geophysical Research*, *110*, 02104. https://doi.org/10.1029/2004ja010649

Koval, A., & Szabo, A. (2008). Modified "Rankine-Hugoniot" shock fitting technique: Simultaneous solution for shock normal and speed. *Journal of Geophysical Research*, *113*, A10110. https://doi.org/10.1029/2008JA013337

Lembège, B., Giacalone, J., Scholer, M., Hada, T., Hoshino, M., Krasnoselskikh, V., et al. (2004). Selected problems in collisionless-shock physics. *Space Science Reviews*, *110*(3/4), 161–226. https://doi.org/10.1023/B:SPAC.0000023372.12232.b7

Mazelle, C., Meziane, K., Le Quéau, D., Wilber, M., Eastwood, J. P., Rème, H., et al. (2003). Production of gyrating ions from nonlinear wave-particle interaction upstream from the Earth's bow shock: A case study from cluster-CIS. *Planetary and Space Science*, *51*(12), 785–795. https://doi.org/10.1016/j.pss.2003.05.002

Němeček, Z., Šafránková, J., Goncharov, O., Přech, L., & Zastenker, G. N. (2013). Ion scales of quasi-perpendicular low-Mach-number interplanetary shocks. *Geophysical Research Letters*, *40*, 4133–4137. https://doi.org/10.1002/grl.50814

Němeček, Z., Šafránková, J., Přech, L., Sibeck, D. G., Kokubun, S., & Mukai, T. (1998). Transient flux enhancements in the magnetosheath. *Geophysical Research Letters*, *25*, 1273–1276. https://doi.org/10.1029/98GL50873

Ofman, L., Balikhin, M., Russell, C. T., & Gedalin, M. (2009). Collisionless relaxation of ion distributions downstream of laminar quasi-perpendicular shocks. *Journal of Geophysical Research*, *114*, A09106. https://doi.org/10.1029/2009JA014365

Ofman, L., & Gedalin, M. (2013). Two-dimensional hybrid simulations of quasi-perpendicular collisionless shock dynamics: Gyrating downstream ion distributions. *Journal of Geophysical Research: Space Physics*, *118*, 1828–1836. https://doi.org/10.1029/2012JA018188

Omidi, N., Sibeck, D., Gutynska, O., & Trattner, K. J. (2014). Magnetosheath filamentary structures formed by ion acceleration at the quasi-parallel bow shock. *Journal of Geophysical Research: Space Physics*, *119*, 2593–2604. https://doi.org/10.1002/2013JA019587

Palmroth, M., Hietala, H., Plaschke, F., Archer, M., Karlsson, T., Blanco-Cano, X., et al. (2018). Magnetosheath jet properties and evolution as determined by a global hybrid-Vlasov simulation. *Annales de Geophysique*, *36*, 1171–1182. https://doi.org/10.5194/angeo-36-1171-2018

Paschmann, G., & Schwartz, S. J. (2000). ISSI book on analysis methods for multi-spacecraft data. In R. A. Harris (Ed.), *Cluster-II Workshop Multiscale/Multipoint Plasma Measurements* (Vol. 449, pp. 99–99). London, UK: ESA Special Publication.

Plaschke, F., & Hietala, H. (2018). Plasma flow patterns in and around magnetosheath jets. *Annales de Geophysique*, *36*, 695–703. https://doi.org/10.5194/angeo-36-695-2018

Plaschke, F., Hietala, H., & Angelopoulos, V. (2013). Anti-sunward high-speed jets in the subsolar magnetosheath. *Annales de Geophysique*, *31*(10), 1877–1889. https://doi.org/10.5194/angeo-31-1877-2013

Plaschke, F., Hietala, H., Angelopoulos, V., & Nakamura, R. (2016). Geoeffective jets impacting the magnetopause are very common. *Journal of Geophysical Research: Space Physics*, *121*, 3240–3253. https://doi.org/10.1002/2016ja022534

Plaschke, F., Hietala, H., Archer, M., Blanco-Cano, X., Kajdic, P., Karlsson, T., et al. (2018). Jets downstream of collisionless shocks. *Space Science Reviews*, *214*, 81. https://doi.org/10.1007/s11214-018-0516-3

Plaschke, F., Karlsson, T., Hietala, H., Archer, M., Vörös, Z., Nakamura, R., et al. (2017). Magnetosheath high-speed jets: Internal structure and interaction with ambient plasma. *Journal of Geophysical Research: Space Physics*, *122*, 10,157–10,175. https://doi.org/10.1002/2017JA024471

Pollock, C., Moore, T., Jacques, A., Burch, J., Gliese, U., Saito, Y., et al. (2016). Fast plasma investigation for Magnetospheric Multiscale. *Space Science Reviews*, *199*(1-4), 331–406. https://doi.org/10.1007/s11214-016-0245-4

Russell, C. T., Anderson, B. J., Baumjohann, W., Bromund, K. R., Dearborn, D., Fischer, D., et al. (2014). The Magnetospheric Multiscale magnetometers. *Space Science Reviews*, *199*(1-4), 189–256. https://doi.org/10.1007/s11214-014-0057-3

Savin, S., Amata, E., Zelenyi, L., Budaev, V., Consolini, G., Treumann, R., et al. (2008). High energy jets in the Earth's magnetosheath: Implications for plasma dynamics and anomalous transport. *JETP Letters*, *87*(11), 593–599. https://doi.org/10.1134/S0021364008110015

Savin, S., Amata, E., Zelenyi, L., Lutsenko, V., Safrankova, J., Nemecek, Z., et al. (2012). Super fast plasma streams as drivers of transient and anomalous magnetospheric dynamics. *Annales de Geophysique*, *30*(1), 1–7. https://doi.org/10.5194/angeo-30-1-2012

Scholer, M., & Burgess, D. (1992). The role of upstream waves in supercritical quasi-parallel shock re-formation. *Journal of Geophysical Research*, *97*(A6), 8319–8326. https://doi.org/10.1029/92JA00312

Schwartz, S. J. (1991). Magnetic field structures and related phenomena at quasi-parallel shocks. *Advances in Space Research*, *11*(9), 231–240. https://doi.org/10.1016/0273-1177(91)90039-M

Schwartz, S. J., Burgess, D., Wilkinson, W. P., Kessel, R. L., Dunlop, M., & Luehr, H. (1992). Observations of short large amplitude magnetic structures at a quasi-parallel shock. *Journal of Geophysical Research*, *97*(A4), 4209–4227. https://doi.org/10.1029/91JA02581

Shue, J.-H., Song, P., Russell, C. T., Steinberg, J. T., Chao, J. K., Zastenker, G., et al. (1998). Magnetopause location under extreme solar wind conditions. *Journal of Geophysical Research*, *103*(A8), 17,691–17,700. https://doi.org/10.1029/98JA01103

Soucek, J., Escoubet, C. P., & Grison, B. (2015). Magnetosheath plasma stability and ULF wave occurrence as a function of location in the magnetosheath and upstream bow shock parameters. *Journal of Geophysical Research: Space*, *120*, 2838–2850. https://doi.org/10.1002/2015JA021087

Vuorinen, L., Hietala, H., & Plaschke, F. (2019). Jets in the magnetosheath: IMF control of where they occur. *Annales de Geophysique*, *37*, 689–697. https://doi.org/10.5194/angeo-37-689-2019

Wilson, L. B., Koval, A., Sibeck, D. G., Szabo, A., Cattell, C. A., Kasper, J. C., et al. (2013). Shocklets, SLAMS, and field-aligned ion beams in the terrestrial foreshock. *Journal of Geophysical Research: Space Physics*, *118*, 957–966. https://doi.org/10.1029/2012ja018186

Yang, Z. W., Lembège, B., & Lu, Q. M. (2012). Impact of the rippling of a perpendicular shock front on ion dynamics. *Journal of Geophysical Research*, *117*, A07222. https://doi.org/10.1029/2011JA017211

Yang, Z. W., Lu, Q. M., Lembège, B., & Wang, S. (2009). Shock front nonstationarity and ion acceleration in supercritical perpendicular shocks. *Journal of Geophysical Research*, *114*, A03111. https://doi.org/10.1029/2008JA013785

Yang, Z. W., Lu, Q. M., & Wang, S. (2009). The evolution of the electric field at a nonstationary perpendicular shock. *Physics of Plasmas*, *16*, 1.